

# A GPS-Based Control Framework for Accurate Current Sharing and Power Quality Improvement in Microgrids

Mohammad S. Golsorkhi, *Student Member, IEEE*, Mehdi Savaghebi, *Senior Member, IEEE*, Dylan D.C. Lu, *Senior Member, IEEE*, J. M. Guerrero, *Fellow, IEEE*, and J. C. Vasquez, *Senior Member, IEEE*

**Abstract**— This paper proposes a novel hierarchical control strategy for improvement of load sharing and power quality in ac microgrids. This control framework is composed of a droop based controller at the primary level, and a combination of distributed power sharing and voltage conditioning schemes at the secondary level. The controllers in the primary level use GPS timing technology to synchronize the local reference angles. The voltage reference of each Distributed Generation (DG) is adjusted according to a voltage-current (V-I) droop characteristic to enable proper current and power sharing with a fast dynamic response. The droop coefficient, which acts as a virtual resistance is adaptively changed as a function of the peak current. This strategy not only simplifies the control design but also improves the current sharing accuracy at high loading conditions. The distributed power sharing scheme uses consensus protocol to ensure proportional sharing of average power. The voltage conditioning scheme produces compensation signals at fundamental and dominant harmonics to improve the voltage quality at a sensitive load bus. Experimental results are presented to validate the efficacy of the proposed method.

**Keywords**— Control, dispersed storage and generation, global positioning system, inverters, power quality

## I. INTRODUCTION

RECENTLY, the concept of Microgrid (MG) as a cluster of Distributed Generators (DGs), energy storage systems and loads has been gaining more interest in the energy research community especially after approval of the IEEE 1547.4 standard [1]. MGs can be connected with the main network or work autonomously as an islanded network.

In case of islanding operation, the local DGs are responsible for load/generation balance and voltage support [2]. Usually, the DGs are coordinated by using the conventional droop strategy. In this method, the frequency and amplitude of the DG reference voltage are computed according to an active power-frequency and reactive power-voltage droop characteristics. The conventional droop method is independent from network topology, does not require any communication network and is simple to implement [3]. However, this method is known to be incompatible with the resistive network impedance, and unbalanced/nonlinear nature of the loads in practical MGs [4]. To alleviate those shortcomings, several

M. S. Golsorkhi (corresponding author) is with the School of Electrical and Information Engineering, The University of Sydney, Darlington, NSW 2006, Australia. (e-mail: MGOL15@yahoo.com). D.D.C. Lu is with the School of Electrical, Mechanical and Mechatronic Systems, University of Technology, Sydney, Ultimo NSW 2007, Australia. He is also with the School of Electrical and Information Engineering, The University of Sydney, Darlington, NSW 2006, Australia. M. Savaghebi, J. M. Guerrero and J.C. Vasquez are with the Department of Energy Technology, Aalborg University, Aalborg, Denmark.

modified droop control methods have been developed [3]-[6], among which virtual impedance-based schemes are the most widely accepted [6].

The virtual impedance schemes achieve a fast dynamic response by modifying the DG voltage according to the DG output current. Furthermore, proper sharing of negative sequence and harmonic currents is achieved by selecting the virtual impedance of each unit inversely proportional with its power rating. However, in weak islanded MG, where the line impedance is considerable, accurate load current sharing requires large virtual impedances which may produce a large voltage distortion [7]. Therefore, there is a trade-off between current sharing accuracy and power quality.

To compensate for the voltage drop on the lines, a virtual capacitance [8] or an adaptive negative virtual resistance [9] can be employed. However, those schemes require the knowledge of line impedances and network topology. An alternative approach is using a hierarchical control structure, composed of primary and secondary levels [10]. The primary controller comprises local DG controllers, which use a combination of droop control method and virtual impedance to coordinate the power generation of DGs and share the harmonic loads between them. The secondary controller produces compensating signals so as to improve the voltage quality in a so-called Sensitive Load Bus (SLB). The compensation signals are broadcasted to the local controllers to adjust the DG reference voltage accordingly. The hierarchical control scheme has been further elaborated in [11] to enhance the frequency regulation. However, the methods of [10] and [11] have some important limitations:

- 1) In order to minimize the communication bandwidth and reduce the adverse effects of communication delays, the voltage of the sensitive load bus is transformed to synchronous rotating frame (dq-frame) and then transformed back to stationary frame ( $\alpha\beta$ -frame) in local controllers. On the other hand, each controller uses the phase angle of its local voltage for Park transformations. Since the voltage angle varies throughout the MG, this process results in transformation errors, which may degrade the performance when the DGs are electrically far. Consequently, current sharing and also voltage quality might deteriorate.

- 2) The selective virtual impedance scheme is not only complex to implement but also suffers from slow dynamics.

- 3) The voltage drop across the lines degrades the performance of virtual impedance scheme in terms of current sharing accuracy. The effect of line impedances can be compensated by means of distributed control techniques as discussed in [12] and [13]-[15]. However, since the secondary

controller is characterized by slow dynamic response, it does not prevent transient overcurrent stresses.

4) The control methods proposed in [10] and [11] are based on the assumption of inductive network impedances. However, the low voltage MGs are mainly resistive in practice.

In this paper, a novel hierarchical control framework, comprised of primary and secondary control levels is proposed to alleviate the aforementioned problems. The main contributions of this paper are as follows:

By extending the voltage-current (V-I) droop concept [16], a new primary control scheme is proposed to achieve accurate current sharing with fast dynamic response. In this method, each DG is synchronized with a common synchronous frame through GPS timing technology. Additionally, the reference voltage is adjusted based on an adaptive V-I droop characteristics to ensure proportional sharing of the load current among the DGs.

While the basic V-I droop method [16] is implemented in the  $dq$  reference frame, the proposed scheme is based on  $abc$  frame to enable fast sharing of harmonic components. Moreover, the droop coefficient is adaptively updated according to the peak current to ensure improved accuracy at high loading conditions. This approach highlights the significance of limiting the peak output current of each DG unit its current ratings.

In contrast with [6], [10], [11], [13-15], [17], which add a virtual impedance to the conventional droop scheme to enable sharing of the harmonic currents, the proposed primary controller integrates the fundamental and harmonic current sharing into a single V-I droop controller. So, the structure of the proposed primary controller is significantly simpler compared to [6], [10], [11], [13-15], [17].

In order to improve the power quality and alleviate the effect of line impedances on the active power sharing, a novel secondary control scheme is proposed. The secondary controller includes a distributed power sharing controller and a centralized voltage conditioning scheme. The distributed power sharing controller acts upon an agent-based structure, in which each agent modifies the d-axis fundamental voltage of the corresponding DG unit according to the difference between the normalized power of the unit and the neighbor units. The voltage conditioning scheme uses a simple integral controller to compensate the voltage deviations and distortions at the SLB.

The rest of the paper is organized as follows. The problem of proportional current sharing in MGs and the conventional solutions are addressed in Section II. The proposed method is introduced in Section III and controller design guidelines are presented in Section IV. Experimental results are presented in Section V. Section VI concludes the paper.

## II. PROPORTIONAL CURRENT SHARING IN ISLANDED MGs

Consider the islanded MG of Fig. 1. The MG includes  $N$  DG units, which are connected to the point of common coupling (PCC) through low voltage lines. The last stage of each DG is a power electronic inverter and a passive LCL filter. The MG supplies a combination of linear/ nonlinear and balanced/unbalanced loads.

The sharing of load current between the DGs is dependent on the output voltages. Therefore, it is possible to achieve proper load sharing by coordinating the output voltages of the individual units. In this section, the conventional current

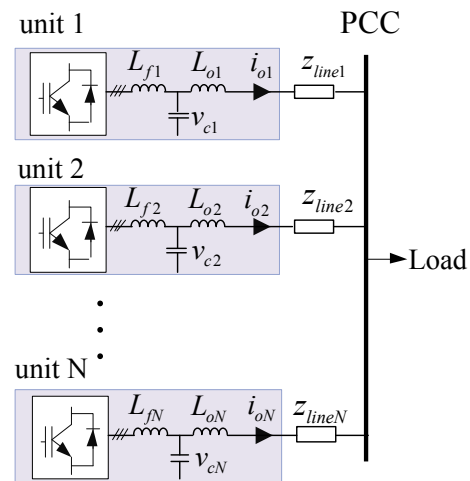


Fig. 1. Schematic diagram of an islanded ac MG.

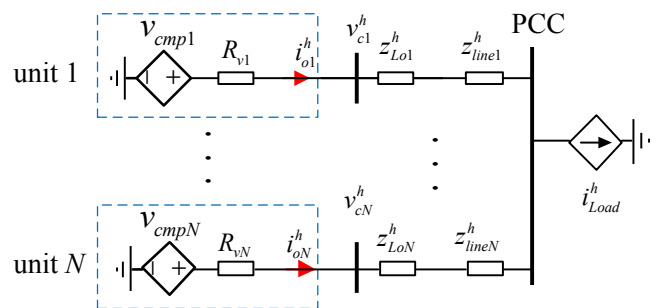


Fig. 2. Equivalent model of the MG for negative sequence and harmonics.

sharing strategies and their shortcomings are discussed.

### A. Virtual resistance scheme

The conventional droop method suffers from several issues including slow dynamics, frequency and voltage fluctuations and degraded sharing accuracy under nonlinear and/or unbalanced loading conditions [2]. One solution for improving the dynamic performance and sharing accuracy is to introduce a virtual resistance in the DG output [6]:

$$v_c^* = E^{1+} - R_v i_o \quad (1)$$

in which  $v_c^*$ ,  $R_v$  and  $i_o$  are the reference voltage, virtual resistance and output current, respectively. Furthermore,  $E^{1+}$  is the fundamental reference voltage obtained from P-V/Q-f droop control method [6]. In order to perform proper current sharing, the virtual impedance of each unit is selected inversely proportional to its power rating:

$$R_{v1} \cdot S_{rated1} = R_{v2} \cdot S_{rated2} = \dots = R_{vN} \cdot S_{ratedN} \quad (2)$$

in which  $S_{ratedk}$  is the rated apparent power of unit k. This scheme is used along with the P-V/Q-f droop method to allow equal sharing of negative sequence and harmonic components.

The effect of virtual resistance on the sharing of harmonic currents can be analyzed based on the equivalent model of Fig. 2. The dynamics of the inner voltage control loop is neglected in this equivalent circuit as its time constant is much smaller compared with the droop controller. Using KVL and KCL, the output current of unit  $k$  is obtained, as follows:

$$i_{ok}^h = \frac{(R_{vk} + z_{ck}^h)^{-1}}{\sum_{i=1}^N (R_{vi} + z_{ci}^h)^{-1}} i_{Load}^h \quad (3)$$

where  $z_{ck}^h = z_{Lok}^h + z_{linek}^h$  and  $z_{Lok}^h$  and  $z_{linek}^h$  are the impedance of output inductor and line of unit  $k$ , respectively. Moreover, the effect of compensation voltage,  $v_{cmp}$ , is neglected.

Comparing (2) and (3), it is observed that the accuracy of current sharing is adversely affected by the output inductor and line impedances. Accurate current sharing necessitates selecting a virtual resistance much larger than  $(z_{ck}^h + z_{linek}^h)$ . On the other hand, the value of virtual resistance is limited by the permissible voltage deviations. Therefore, the sharing accuracy of the virtual resistance method might be poor in practice [18].

### B. Selective virtual impedance scheme

Since the fundamental power factor is higher than 0.7 in practice, the fundamental voltage deviations caused by a virtual resistance is higher compared with a virtual inductance with the same impedance. In order to attain a desirable voltage regulation while taking advantage of the improved damping of the virtual resistance, the virtual impedance scheme is adopted. In this method, the reference voltage corresponding to harmonic order  $h$  ( $h=1+,1-,2+,2-,...$ ) is defined as

$$v_c^{h*} = E^h - Z_v^h i_o^h \quad (4)$$

in which  $E_k^h$  is equal to  $E_k^{1+}$  for the fundamental positive sequence component and zero, otherwise. Moreover,  $Z_v^h$  is the virtual impedance matrix, which is defined as

$$Z_v^h = \begin{bmatrix} R_v^h & -X_v^h \\ X_v^h & R_v^h \end{bmatrix} \quad (5)$$

This virtual impedance method is commonly implemented in  $\alpha\beta$  reference frame. The main challenge for implementation of the virtual impedance scheme is extraction of the  $\alpha\beta$  components corresponding to each of the dominant harmonics. A straightforward solution for is transforming the signal to the synchronous rotating reference frame (SRRF) rotating with angular speed of  $h\omega_0$ , averaging the  $d$  and  $q$  components of the signal to remove the other components and transforming the averaged components back to the  $\alpha\beta$  frame [11]. However, the averaging filters incur a delay, which slows down the current sharing dynamics. In order to improve the current sharing dynamics, a multi-resonant frequency-locked loop harmonic extraction method is proposed in [19]. Nonetheless, this method is complex and computationally expensive.

### C. Effect of harmonic compensation on current sharing

The voltage drops across the virtual impedance, DGs output inductors and the lines give rise to voltage distortions at the PCC. In order to improve the quality of voltage, secondary harmonic compensation schemes are adopted [10], [11], [15], [17]. In these methods, a secondary controller calculates a compensation command for each of the dominant harmonics. The compensation commands are broadcasted to the local controllers via a communication network. Based on the received commands, each local controller adds a compensation voltage to its output voltage.

To reduce the communication bandwidth, the compensation commands are broadcasted in the form of  $d$  and  $q$  components.

This necessitates the utilization of Park and inverse Park Transformations at the secondary and local controllers, respectively. Such transformations cause an error in the received compensation command due to the mismatch between the reference angles of the secondary and local controllers.

The effect of transformation error on the current sharing among the DGs can be analyzed based on the MG model of Fig. 2. To simplify the analysis, it is assumed that the compensation command is directly injected into the reference voltage of the inverter and  $N=2$ . The compensation signal computed at local controller  $i$ ,  $v_{cmpi}^h$ , is related with the secondary controller command,  $v_{cmp}^h$ , as follows:

$$\begin{bmatrix} v_{cmpi,d}^h \\ v_{cmpi,q}^h \end{bmatrix} = \begin{bmatrix} \cos(h\delta_i) & \sin(h\delta_i) \\ -\sin(h\delta_i) & \cos(h\delta_i) \end{bmatrix} \begin{bmatrix} v_{cmp,d}^h \\ v_{cmp,q}^h \end{bmatrix} \quad (6)$$

in which  $\delta_i$  is the difference between the reference angle of the local controller  $i$  ( $\theta_{refi}$ ) and the secondary controller ( $\theta_{refs}$ ):

$$\delta_i = \theta_{refi} - \theta_{refs} \quad (7)$$

It should be pointed out the angles  $\theta_{refi}$  and  $\theta_{refs}$  are conventionally extracted from the local voltages by means of a PLL [10], [11], [15], [17]. Therefore, an unintentional mismatch exists between  $\theta_{refi}$  and  $\theta_{refs}$  due to the line impedances. As a result, the compensation voltages of each local controller varies depending on the corresponding voltage angle and the harmonic order. From Fig. 2, the current of unit 1 is calculated using superposition theorem as shown in (8).

$$i_{o1}^h = \frac{R_{v2} + z_{c2}^h}{\sum_{i=1}^2 (R_{vi} + z_{ci}^h)} i_{Load}^h + \begin{bmatrix} \cos(h\delta_1) - \cos(h\delta_2) & \sin(h\delta_1) - \sin(h\delta_2) \\ -\sin(h\delta_1) + \sin(h\delta_2) & \cos(h\delta_1) - \cos(h\delta_2) \end{bmatrix} \frac{v_{cmp}^h}{\sum_{i=1}^2 (R_{vi} + z_{ci}^h)} \quad (8)$$

Equation (8) implies that the transformation error alters the current sharing between the units. Moreover, the effect of transformation error is escalated at higher order harmonics. This unintentional and uncontrolled issue might cause circulating harmonic currents among the units and expose some units to overcurrent stresses under high loading conditions. In Section III, a solution is proposed to tackle this problem.

## III. PROPOSED CONTROL METHOD

In order to improve the current sharing accuracy in islanded MGs while ensuring high power quality, a novel control strategy is proposed in this paper. The proposed control method for a general MG consisting of  $N$  voltage-controlled DGs and several loads, which can be balanced, unbalanced, linear or nonlinear is depicted in Fig. 3. The control framework is comprised of primary and secondary control levels. At the primary level, a new droop controller is proposed to enable sharing of load current among the DG unit with a fast dynamic response. The secondary control level includes a centralized voltage conditioning module and distributed power sharing control agents. The individual control agents and the voltage conditioning module are interconnected through a low bandwidth communication (LBC) network. Additionally, the

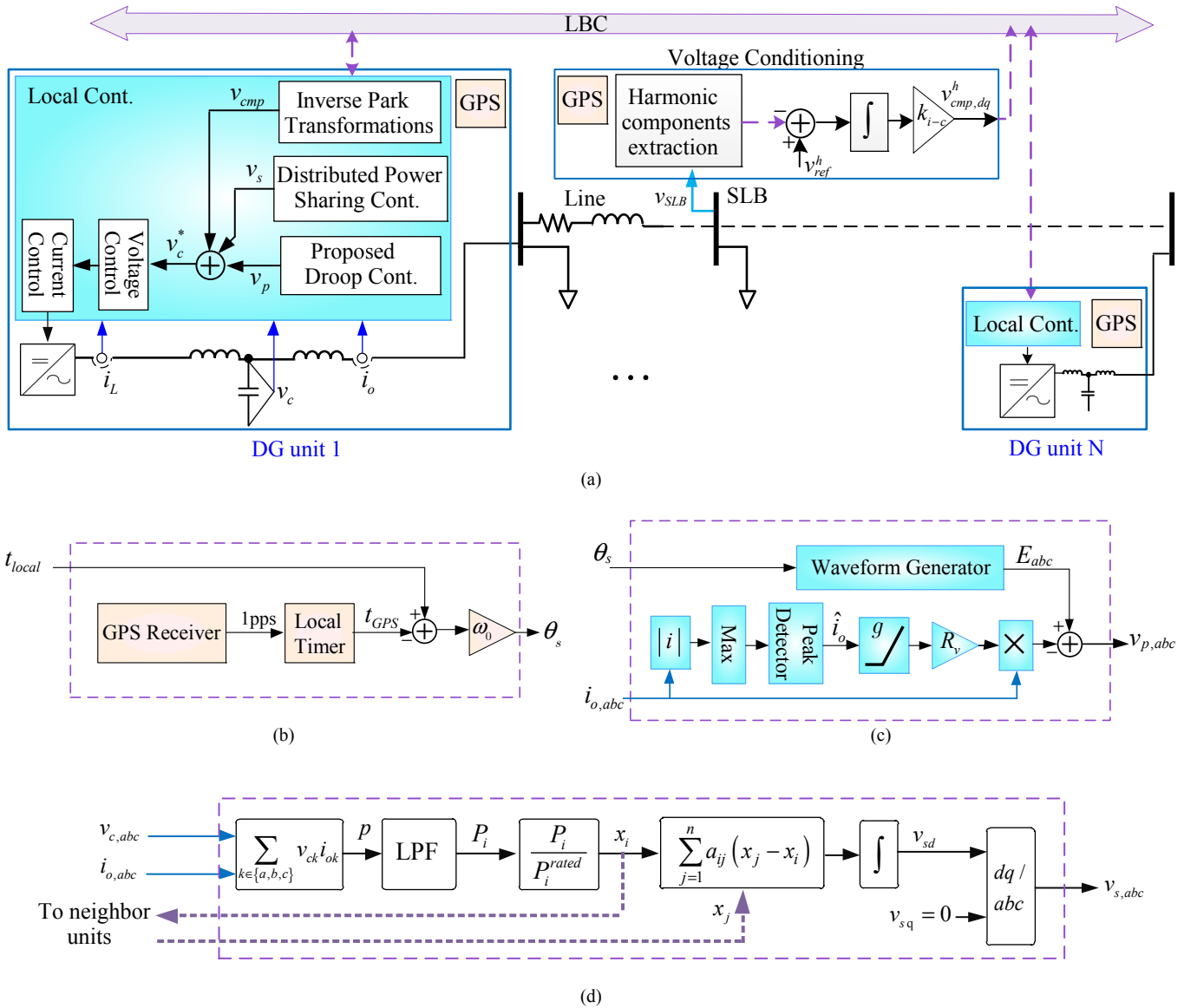


Fig. 3. Proposed control framework. a) Control layout, b) GPS timing, c) Droop controller and d) Distributed secondary controller.

DG units are synchronized by GPS timing technology.

The inverter reference voltage is obtained as the summation of the droop and secondary control signals. A cascaded control scheme comprising Proportional-Resonant (PR) voltage and current controllers is used in the inner control loop to track the reference voltage [20].

#### A. GPS-based time synchronization

GPS synchronization is widely known for its application in Phasor Measurement Units (PMUs) for high voltage power systems [21]. Over the recent years, however, GPS technology has been also used in small scale applications. Particularly, low cost micro-synchrophasors ( $\mu$ PMUs), have been suggested for smart-home measurement systems [22]. Additionally, several GPS based control schemes have been proposed for MG applications [23]-[28]. In comparison with the conventional droop method, GPS-based approaches favor from fixed frequency operation but also simple and smooth connection of individual units [29]. In the proposed method, GPS technology provides additional advantages. Specifically,

- As detailed in Section II-C, the PLL-based synchronization gives rise to Park transformation errors in the secondary

control layer. Therefore, the accuracy of harmonic current sharing might degrade. This issue can be resolved by using GPS, which provides a global reference angle for secondary and local controllers.

- With GPS synchronization, all units can be coordinated with a common SRRF. In this context, voltage-current droop characteristics can replace the conventional P-f and Q-E droop characteristics [30]. Hence, faster and more accurate current sharing can be achieved.

A GPS receiver calculates its three dimensional position as well as the offset between its local time and Universal Coordinated time (UTC) by comparing the time delay of the signals received from 4 of the GPS satellites. A 1 pulse per second (1-pps) signal is then generated, the rise time of which is in synchronism with the UTC. The 1-pps signal can be used as a time reference for synchronizing several distributed units. The schematic diagram of the GPS timing block is illustrated in Fig. 3 (b). As seen, the rise time of the 1-pps signal generated by the GPS receiver is captured by the timer module of the local controller. The difference between the captured time,  $t_{GPS}$ , and the local time,  $t_{local}$ , is multiplied by the fundamental frequency,  $\omega_0$  to obtain the reference angle of the local SRRF,  $\theta_s$ . Since the

1-pps signals generated by each GPS receiver unit are synchronized with the UTC, the reference angle of each local controller is synchronized with a global SRRF.

In the ideal case that the frequency of local oscillator is fixed at nominal value, a single GPS pulse is enough to indefinitely align the local time with the UTC. In practice, however, the oscillator frequency drifts due to temperature variations and aging [31]. That is the reason a 1-pps signal is used to repeat the process of the time alignment each second. It should be highlighted that the low rate of the GPS signal is in accordance with small frequency drift of off-the-shelf oscillators. As detailed in [29], the accuracy of GPS-based synchronization is less than 1° with for a typical oscillator frequency drift of around 1 part per million.

In case of GPS signal interruption, the local time gradually deviates from the UTC. Therefore, the current sharing is degraded and in the long term and the system might become unstable. This problem can be solved by using an adaptive Q-f droop controller as a backup for GPS synchronization in [29].

### B. Droop control strategy

In this section, a new decentralized control method as an extension for V-I droop concept [16] is proposed to enable fast and accurate current sharing. In this method, the primary control action of unit  $k$  is defined according to the following adaptive voltage-current droop law:

$$v_{pk,abc} = E_{0abc} - r_{vk} (\hat{i}_{ok}) i_{ok} \quad (9)$$

in which  $r_{vk}$  is the adaptive virtual resistance, which is adjusted according to the largest peak of the  $abc$  output currents,  $\hat{i}_{ok}$ . Furthermore, the no-load reference voltage,  $E_{0abc}$ , is a balanced sinusoidal voltage with rated amplitude and frequency:

$$E_{0abc} = \begin{bmatrix} E_0 \sin \theta_s & E_0 \sin(\theta_s - \frac{2\pi}{3}) & E_0 \sin(\theta_s - \frac{4\pi}{3}) \end{bmatrix}^T \quad (10)$$

Equation (10) implies that the phasor of the no-load voltage set point is aligned with the  $d$  axis of the global SRRF.

The proposed droop controller provides a simple and unified droop scheme for sharing of fundamental active and reactive power as well as harmonic components. The salient feature of the proposed droop method is the emphasis on the accurate sharing of instantaneous current instead of power (conventional droop [32]) or  $d$  and  $q$  components of current (basic V-I droop [16]).

The adaptive virtual resistance is defined as

$$r_{vk} (\hat{i}_{ok}) = R_{vk} g (\hat{i}_{ok}) \quad (11)$$

in which  $R_{vk}$  is the maximum virtual resistance, which is selected based on the maximum permissible voltage deviations. Moreover,  $g$  is a monotonic piecewise linear function with a maximum value of 1.

The mechanism of operation of the proposed droop method is explained based on the model of Fig. 2. Consider a MG composed of two DG units with equal power ratings. Using current division rule, the output current of unit 1 is expressed as

$$i_{o1}^h = \frac{(r_{v2} + z_{c2}^h)}{(r_{v2} + z_{c2}^h) + (r_{v1} + z_{c1}^h)} i_{Load}^h, \quad (12)$$

Substituting (11) into (12) and rearranging the terms, the following expression is obtained:

$$i_{o1}^h = \frac{1}{2} i_{Load}^h + \frac{g(\hat{i}_{o2}) - g(\hat{i}_{o1}) + \frac{z_{c2}^h - z_{c1}^h}{R_v}}{g(\hat{i}_{o1}) + g(\hat{i}_{o2}) + \frac{z_{c1}^h + z_{c2}^h}{R_v}} i_{Load}^h, \quad (13)$$

Ideally, the load current is shared equally between the units and the second term on the Right Hand Side (RHS) of (13) is zero. In practice, however, the mismatch between the line impedances gives rise to the sharing error. By using the presented adaptive virtual resistance, if the peak current of unit 1 is larger than unit 2, the term  $g(\hat{i}_{o2}) - g(\hat{i}_{o1})$  goes negative, hence reducing the current of unit 1. Otherwise,  $g(\hat{i}_{o2}) - g(\hat{i}_{o1})$  goes positive, thus increasing the current of unit 1. Therefore, the proposed scheme improves the current sharing accuracy compared to the conventional virtual resistance method. Additionally, the sharing accuracy is improved at higher loading conditions due to the higher slope of the function  $g$ . This way, the DGs are protected from overcurrent stresses without imposing additional voltage distortion. It is worth mention that although the increase of  $r_{vk}$  causes higher voltage distortion at high loading conditions, since  $g_{max}=1$ , the maximum distortion is the same as the fixed resistance case.

The block diagram of the proposed droop scheme is depicted in Fig. 3 (c). An absolute value block followed by a max block detects the phase with the largest instantaneous magnitude of current. A classic peak detector [33] then extracts the largest peak of the output currents. The adaptive virtual impedance is calculated according to (11) and multiplied by the instantaneous currents to obtain the virtual resistance voltage drop. Finally, the primary control action is achieved by subtracting the virtual resistance drop from the no-load voltage.

### C. Distributed power sharing controller

The adaptive droop method proposed in Section III-B, resolves the challenge of accurate load sharing at high loading conditions to prevent overloading. However, it might be technically or economically desirable to accurately share the active power at low/medium loading conditions as well. To achieve this objective, a novel distributed power sharing control method is proposed in this section.

Assuming the output voltage is aligned with the  $d$ -axis, the active power is proportional to the  $i_{od}^{1+}$ . On the other hand, due to the resistive nature of the network impedance,  $i_{od}^{1+}$  is dependent on the  $v_{cd}^{1+}$ . Therefore, it is possible to modify the active power dispatch by altering  $v_{cd}^{1+}$  of the individual units.

The operation of the power sharing controller for a MG comprising of two DG units is illustrated in Fig. 4. For simplicity, the DGs are assumed identical and the impedance of line 2 is assumed zero. In Fig. 4 (a), the voltage correction terms are zero. So, both DG1 (solid line) and DG2 (broken line) droop characteristics start from  $E_0$  and drop with a rate of  $r_v$ . However, due to the voltage drop on line 1, the voltage of DG1 is higher. As a result, DG1 supplies a smaller current compared to DG2. In case of Fig. 4 (b), a negative voltage correction term is applied to DG2. As a result, the droop characteristic of DG2 is shifted down and even current sharing is achieved.

The schematic diagram of the power sharing controller is illustrated in Fig. 3 (d). In order to achieve proportional power sharing among the units, the voltage correction term for DG

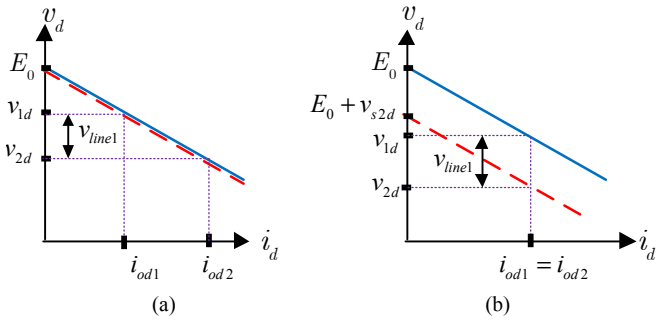


Fig. 4. Sharing of d-axis current among two DGs. a) Before and b) after adding the voltage correction.

unit  $i$  is updated based on the consensus protocol [34]. In this method, each local controller is regarded as a control agent. The information state of agent  $i$ ,  $x_i$  is defined as the normalized active power of the unit:

$$x_i = P_i^{norm} = \frac{P_i}{P_i^{rated}} \quad (14)$$

in which  $P_i$  and  $P_i^{rated}$  refer to the total (fundamental plus harmonic) active power and rated power of unit  $i$ , respectively. The information states are shared between the agents, through a sparse communication network. The state of each agent is updated based on the received information from the neighbors,

$$v_{si,d} = \int_0^t \sum_{j=1}^n a_{ij} (x_j(\tau) - x_i(\tau)) d\tau \quad (15)$$

in which the communication weight,  $a_{ij}$ , is a constant positive number if agent  $i$  receives information from agent  $j$  and zero, otherwise. If the distributed communication network contains minimum connectivity, all of the states will converge to a common value:  $x_0 = x_1 = \dots = x_n$  [35]. In other words, the load active power will be proportionally shared among the DGs.

#### D. Voltage conditioning module

As shown in Fig. 3 (a), the voltage conditioning module is composed of a harmonic extraction block and an integral controller. The harmonic components of the SLB voltage are extracted according to the method proposed in [36]. The compensation signal corresponding to harmonic order  $h$ ,  $v_{cmp}^h$ , is then computed by means of an integral controller, as follows:

$$v_{cmp,d}^h = k_c \int (v_{refd}^h - v_{SLBd}^h) dt \quad (16)$$

$$v_{cmp,q}^h = k_c \int (v_{refq}^h - v_{SLBq}^h) dt \quad (17)$$

in which  $k_c$  and  $v_{SLB}^h$  are the integral controller gain and component  $h$  of the SLB voltage, respectively. In order to regulate the fundamental voltage at the rated value and eliminate the harmonic distortions, the reference voltage,  $v_{ref}^h$  is set as  $v_{refd}^1 = E_0$ ,  $v_{refq}^1 = 0$  for fundamental component and zero for other components. The compensation signals are broadcasted to the DGs. At the DG level, the compensation voltage is transformed back to the  $abc$  frame and injected to the DG reference voltage.

Since all of the local controllers are synchronized by means of GPS technology, the Park / inverse Park transformation errors, which are addressed in Section II-C are eliminated.

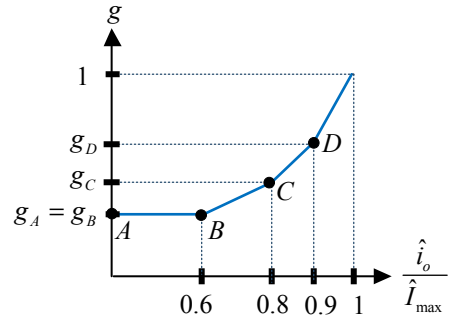


Fig. 5. Adaptive virtual resistance function.

Therefore, all DG units exert an identical compensation voltage, and the current sharing remains unchanged.

#### IV. CONTROLLER DESIGN

The maximum instantaneous voltage deviation,  $\Delta \hat{v}_{max}$ , following a step load change is related to  $R_v$  as:

$$\Delta \hat{v}_{max} = R_v \hat{i}_{o,max} \quad (18)$$

Assuming a maximum step load change of 1pu and a maximum voltage deviation of 10%, the maximum virtual resistance is selected as 0.1pu. According to the small signal analysis presented in [16] and [29], a virtual resistance of 0.1pu also satisfies the stability criterion.

The function  $g$  is designed considering the following points:

- 1- To improve the current sharing accuracy at higher loading conditions,  $g$  should be monotonically increasing.
- 2- To simplify the implementation, a piecewise linear characteristic is adopted.
- 3- The minimum value of  $g$  is selected so as to achieve a reasonable sharing accuracy at low loading conditions.
- 4- The function is normalized.

The design of the piecewise linear function  $g$  involves the selection of a set of breakpoints. In this paper, the breakpoints are selected at 0%, 60%, 80%, 90% and 100% loading.

The function  $g$  is illustrated in Fig. 5. For the low loading region, the function is constant. The coordinates of the breakpoints can be denoted as with the following: A (0,  $g_B$ ), B (0.6,  $g_B$ ), C (0.8,  $g_C$ ), D (0.9,  $g_D$ ), E (1, 1). Intuitively, the parameters  $g_B, g_C, g_D$  should be selected such that the function  $g$  has a higher slope at higher loading conditions. A systematic design method is to select  $g_B, g_C, g_D$  by solving the following offline optimization problem:

$$\min Cf = \sum_{x \in \{A,B,C,D\}} C_x e_x \quad (19)$$

$$st. g_A = g_B, \quad (20)$$

$$g_E = 1, \quad (21)$$

where  $Cf$  is the cost function,  $C_x$  is the penalty factor corresponding with loading condition  $x$  ( $x=A,B,C,D$ ) and  $e_x$  is current sharing error at point  $x$ . The cost function, which is a merit for the sharing accuracy, is defined as the weighted sum of the current sharing error at each of the loading points. By selecting a larger penalty factor (weight) for higher loading conditions, the prominence of improved sharing accuracy at high load currents is highlighted. Here, penalty factors are selected as  $C_A = 1$ ,  $C_B = 2$ ,  $C_C = 4$ ,  $C_D = 16$ .

The optimization problem (19)–(21) is solved numerically

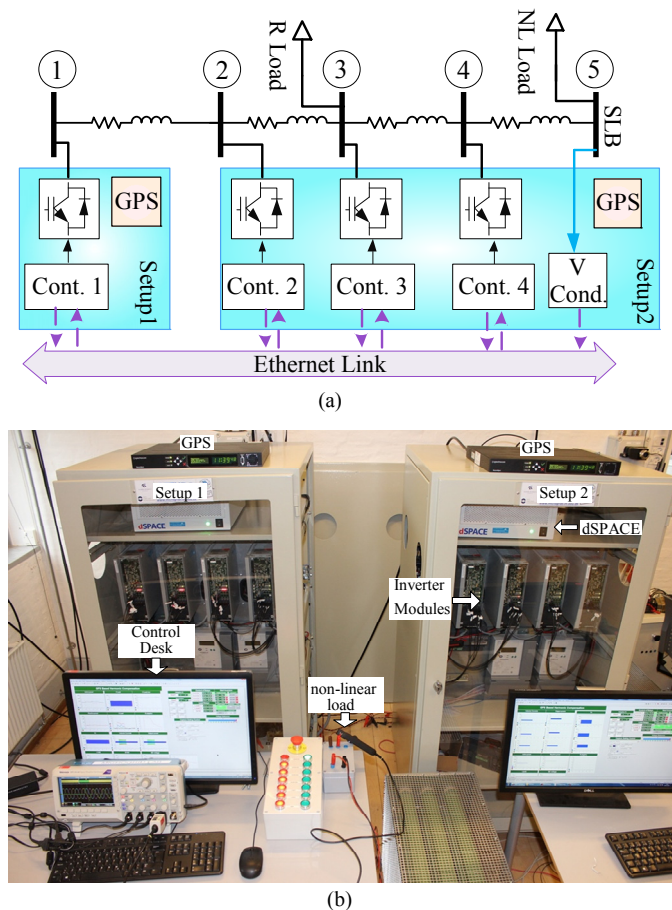


Fig. 6. Test microgrid: a) schematic diagram, and b) Photo of the setup.

by using direct search method [37]. In this method, each of the variables  $g_B$ ,  $g_C$ ,  $g_D$  are discretized with steps of 0.01 the interval [0,1]. For each of the possible combinations, the function  $g$  is constructed and the current sharing error corresponding to points A, B, C and D is calculated according to (13). Then, the cost is obtained from (19). The optimum solution, i.e., the combination with the lowest cost is found as:  $g_B = 0.33$ ,  $g_C = 0.46$  and  $g_D = 0.62$ . Thanks to the small number of variables, the computation time for obtaining the solution is as short as a few seconds on a core i5 PC.

The peak detector instantaneously increases the adaptive virtual resistance during step load rises. When the load drops, however, the virtual resistance drops with a time constant  $\tau$ . The parameter  $\tau$  must be much larger than the time constant of the droop controller as well as the period of the peak current signal to decouple the dynamics of the droop controller from the peak detector and ensure smooth variations of the virtual resistance. On the other hand, the peak detector must be fast enough to allow the virtual resistance settle at steady-state before the next load rise. The designing of inner control loops and the secondary controller has been addressed in [10], [38], [39].

## V. EXPERIMENTAL RESULTS

The proposed method has been implemented on a laboratory scale test bed illustrated in Fig. 6. The test bed was prototyped in the Microgrid Laboratory at Aalborg University [40]. The test bed includes four DG units and two loads interconnected through resistive line models. Each DG unit is composed of a 2.2kW inverter followed by an LCL filter. A programmable DC

TABLE I. PARAMETERS OF THE TEST MG

Description	Parameter	Value	Unit
Fundamental frequency	$f_0$	50	Hz
Rated phase voltage	$V_{rated}$	220	Vrms
Inverter specifications	$I_{peak,max}$	5	A
	$f_{PWM}$	10	kHz
LCL filter	$L_f$	8.6	mH
	$C_f$	4.5	$\mu$ F
	$L_o$	1.8	mH
Resistive load	$R_l$	57	$\Omega$
Nonlinear load (DC side)	$R_{NL}$	130	$\Omega$
	$C_{NL}$	115	$\mu$ F
Line impedances	$Z_{line1-2}$	$0.22+j0.03$	$\Omega$
	$Z_{line2-3}$	$0.22+j0.03$	$\Omega$
	$Z_{line3-4}$	$0.5+j0.06$	$\Omega$
	$Z_{line4-5}$	$0.5+j0.06$	$\Omega$
Communication rate	$f_{com}$	100	Sample/s
Communication delay	$T_{dcom}$	10	ms
V-I droop	$R_v$	6	$\Omega$
	$\tau$	1	s
Power controller gain	$a_{ij}$	50	V/s
Voltage conditioning gain	$k_c$	5	1/s

power source supplies the inverters. The MG supplies a linear balanced load as well as a nonlinear unbalanced load, which is comprised of a single phase rectifier connected between phase  $a$  and  $b$ . This MG was assembled based on two experimental setups. Each of the setups is equipped with a Securecync ® GPS receivers from Spectracom and a dSPACE 1006 digital control platform. An Ethernet communication link is used for broadcasting the secondary controller signal to the local controllers. Each of the dSPACE controllers are connected to a desktop PC, which uses the “dSPACE Control Desk” program for management of the dSPACE signals and commands. The experimental results (except SLB voltage) are captured using the “dSPACE control desk” and plotted in MATLAB.

The specifications of the test bed as well as the control parameters are listed in Table I. The LCL filter is designed based on the procedure proposed in [41]. To reduce inverter losses, the maximum switching ripple current is selected as 20% of the nominal current, i.e., 1A. As a result, the converter side inductance ( $L_f$ ) is calculated as  $0.04\mu$ H ( $\approx 8.6$ mH) [42]. In order to reduce the output current ripple while maintaining the capacitor reactive power below  $0.1\mu$ H, the filter capacitor ( $C_f$ ) is selected as  $0.1\mu$ F ( $\approx 4.5\mu$ F). Finally, assuming a desirable output current ripple of 1%, the output inductance ( $L_o$ ) is calculated as 1.8 mH [41]. The load impedances are selected so that the full load current is close to the inverters rated power. The R/X ratio of lines is selected around 7 to mimic typical low voltage feeders [43]. To model a low bandwidth communication link, the data rate is limited to 100 sample/s and an intentional delay of 10 ms is introduced for each of the links. The performance of the MG is investigated under seven case studies.

### A. Effect of adaptive virtual resistance and secondary control

In the first case, the effect of the proposed adaptive droop function and secondary controller on the current sharing accuracy and power quality is studied. The experimental results for this case are shown in Fig. 7. Prior to  $t=3$ s, a fixed virtual resistance is adopted by setting the droop function in equation

(11), equal to 1. From Fig. 7(a), it is observed that P1, P2, P3, and P4 are 910 W, 960 W, 1020W, 1050W, respectively. Therefore, the DGs which are electrically closer to the load pick up a larger share from the load. The sharing error is also reflected in peak current, as shown in Fig. 7(b). The rms voltages at the SLB are within the standard range of 0.95pu to 1.05pu thanks to the smart selection of the virtual resistance. However, as shown in Fig. 7(e), the SLB voltage quality is degraded. Particularly, the unbalance factor (UF) is at 2.7%, and the positive and negative sequence components of the third harmonic (H3+ , H3-) are at around 1.7%. Furthermore, the positive and negative components of the fifth harmonic (H5+,H5-) are at around 0.6%, respectively. It is worth mentioning that the higher order harmonics are negligible, hence are not shown for brevity.

Around  $t=3s$ , the adaptive virtual resistance is activated. As shown in Fig. 7 (c), the DGs which are electrically closer to the load adopt a larger virtual resistance. This way, the adverse effect of line impedances on current sharing accuracy is reduced. As a result, the load sharing accuracy is improved, as depicted in Fig 7(b).

Around  $t=6s$ , the secondary controller is activated to regulate the SLB voltage is regulated at 1pu and eliminate the voltage distortions. The harmonic compensation results in an increase of the load current, which in turn causes the DG currents to increase. Consequently, the adaptive virtual resistances are increased to improve the sharing accuracy (See Fig. 7(c)).

### B. Step load response

In the cases 2,3,4,6 and 7 the nonlinear load is switched on and off to study the step load response. The second case study examines the performance of conventional method based on power droops, which is discussed in Section II-A. The control parameters for the second scenario are listed in Table II. The droop coefficients are designed based on the eigenvalue analysis [16] and the virtual resistance is selected so as to limit the voltage within 0.95-1.05pu.

The experimental results for the case 2 are illustrated in Fig. 8. As shown in Figs. 8(a) and (c), DG unit 4, which is electrically closer to the nonlinear load, supplies the largest share of active power (P4) and current (I4) followed by units 3, 2, and 1. Because reactive power coordination is conducted based on frequency, which is a global parameter as opposed to voltage, Q sharing is accurate (see Fig. 8(b)). Nevertheless, the current sharing is inaccurate, which results in I4 exceeding the rated value (5A). As shown in Fig. 8 (d), the SLB voltage is distorted following the connection of the nonlinear load. As a consequence, the third and fifth harmonic of line *ab* are increased to 2.8% and 1.2%, respectively (See Fig. 8 (e)). Furthermore, the THD is around 3.2%, 1.5% and 1.8% for lines *ab*, *bc* and *ca*, respectively.

In the third case, the step load change response of the proposed droop method without secondary control layer is investigated. The experimental results for the case 3 are illustrated in Fig. 9. Comparing Fig. 8(c) and 9(c) reveals the improved current sharing accuracy of the proposed droop method. The enhanced current sharing is achieved by adaptive adjustment of virtual resistances according to the output current. Specifically, the virtual resistance of unit 4 is increased above other units, which results in the decrease of P4 below P3

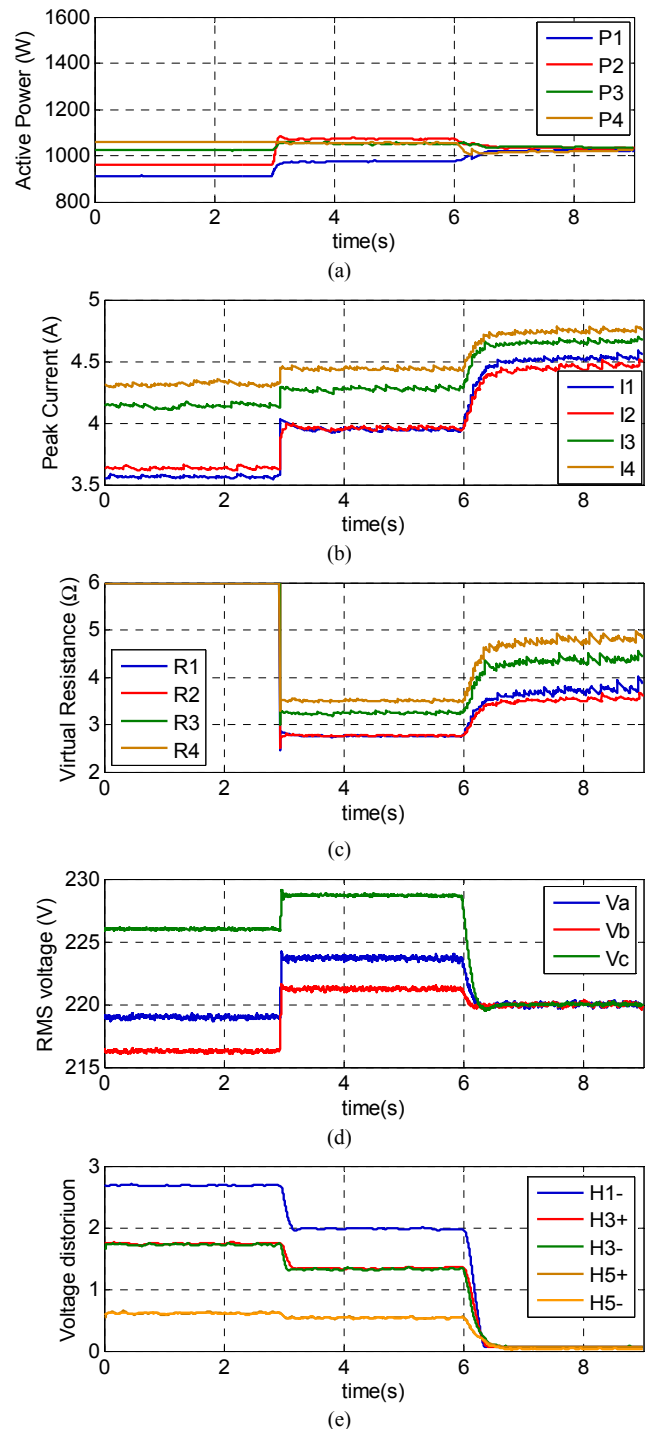


Fig. 7. Experimental results for the first study: a) active power, b) peak current, c) virtual resistance, d) SLB RMS voltage, and e) SLB harmonics.

TABLE II. CONTROL PARAMETERS OF THE VIRTUAL RESISTANCE METHOD

Description	Value	Unit
P-V droop coefficient	0.0075	V/W
Q-f droop coefficient	0.00001	Hz/W
Virtual resistance	3	$\Omega$

and P2 (see Fig. 9(a)). As shown in Fig. 9 (b), although reactive power sharing is not ideal, the sharing error is less than 0.01pu. Moreover, the voltage harmonics are almost the same as the conventional method, as shown in Figs. 9 (d) and (e).

In the fourth case, the proposed method with secondary control layer is tested. The experimental results for this case are shown in Fig. 10. Comparison of Fig. 9 (a) and 10 (a) reveals



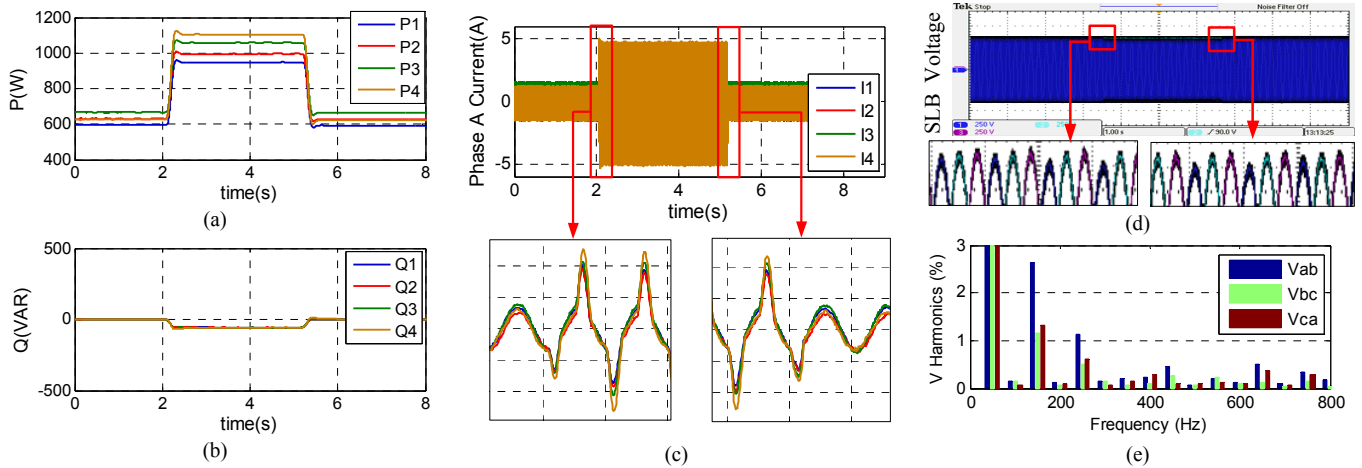


Fig. 8. Step load response of the conventional method: a) Active power, b) Reactive power, c) DG currents, d) SLB voltage, and e) Voltage harmonics.

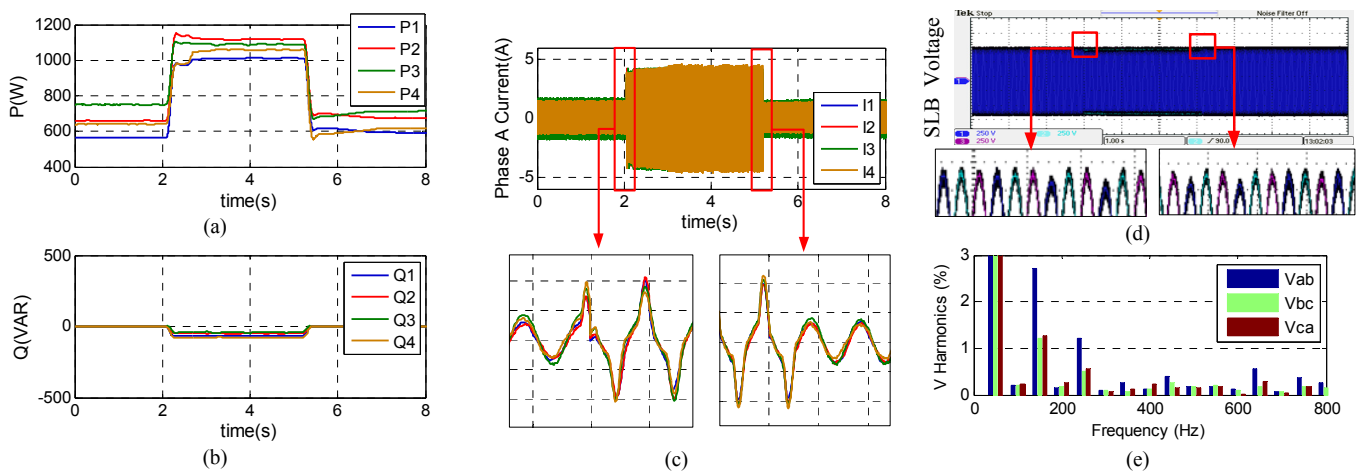


Fig. 9. Step load response of the proposed droop method without secondary control: a) Active powers, b) Reactive powers, c) Phase *a* currents, d) SLB voltage, and e) Voltage harmonics.

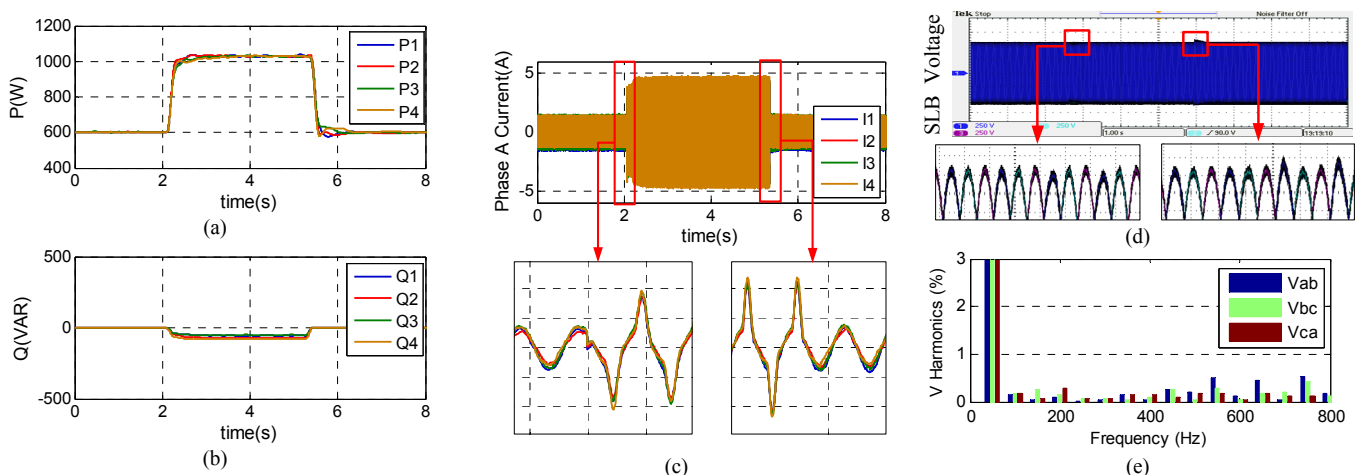


Fig. 10. Step load response of the proposed method: a) Active powers, b) Reactive powers, c) Phase *a* currents, d) SLB voltage, and e) Voltage harmonics.

that the secondary controller improves the accuracy of active power sharing. Since the dynamics of the secondary control layer are relatively slow, the SLB voltage experiences transient distortions following the load changes (see Fig. 10 (d)). However, the instantaneous voltages are within the permissible range of 0.95pu to 1.05pu. Furthermore, as shown in Fig. 10 (e), the third and fifth harmonics of the SLB voltage are eliminated in the steady-state. As a result, the voltage THD corresponding to lines *ab*, *bc* and *ca* is reduced from 3.3%, 1.5% and 1.8% in the third case to 1 %, 0.8% and 0.85%, respectively.

### C. Plug and play operation

The fifth study demonstrates the Plug and Play (P'n'P) feature of the proposed strategy. In this scenario, the DG unit 4 is disconnected from and reconnected to the MG at  $t=1s$  and  $t=6.5s$ , respectively. As shown in Fig. 11 (a) and (b), following the outage of unit 4, the power and current of units 1-3 are increased to maintain the load/generation balance. Although unit 4 is electrically disconnected from the MG but its voltage remains synchronized with the grid thanks to the GPS

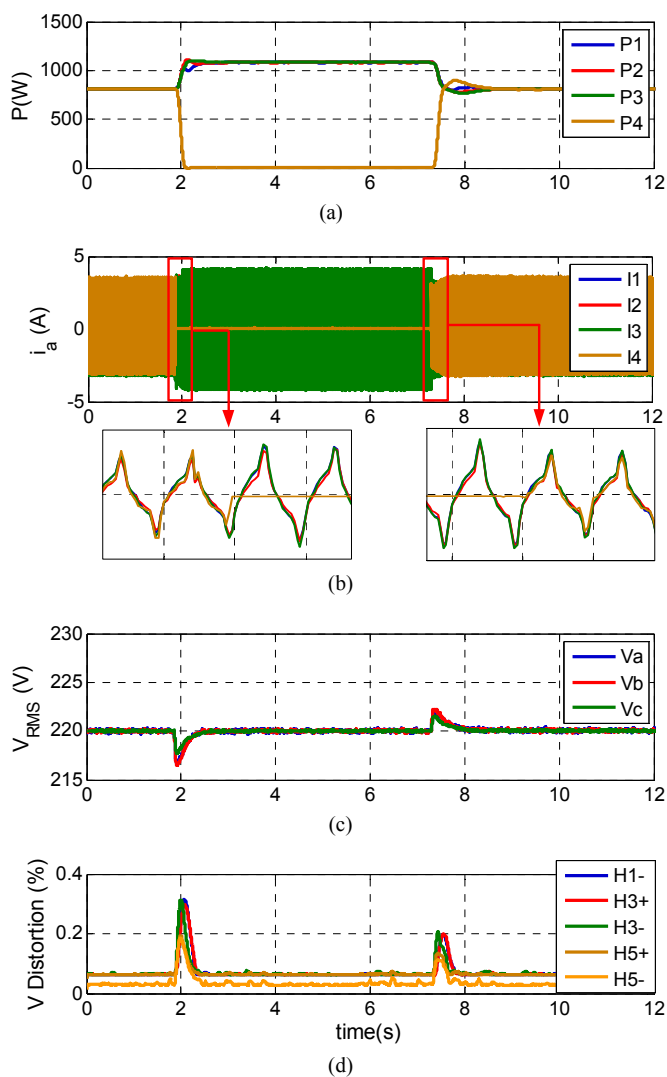


Fig. 11 Response of the proposed method to outage and reconnection of unit 4: a) active powers, b) currents, and c) RMS voltage and d) harmonic distortion.

synchronization technology. This facilitates the reconnection of unit 4 and ensures a smooth reconnection. From Fig. 11 (c) and (d) it is observed that the voltage deviation and harmonic distortion exhibit a small increase during the transients but are changed back to zero within less than a second.

#### D. Effect of network impedance

Although the proposed droop control method is developed for MGs with low X/R ratio, it is also applicable to the MGs with inductive network impedance. In the sixth case, the effect of network X/R ratio on the current sharing accuracy is investigated by performing the step load change test under the following conditions: 1) lines are modeled by  $0.22\Omega$  resistors, 2) lines are modeled by  $0.5\text{mH}$  inductors. The experimental results for the resistive and inductive line cases are shown in Fig. 12. It is observed that in case of inductive network, I4 contains more distortion compared to other units. The reason is the degraded current sharing accuracy at high order harmonics due to the larger line impedance at higher frequencies. Nevertheless, the peak current of all units are almost the same in both resistive and inductive cases. Therefore, overcurrent stresses are prevented regardless of the network X/R ratio. From Figs. 12 (b) and (d), it is observed that in both cases the inverter voltages are regulated around the rated value.

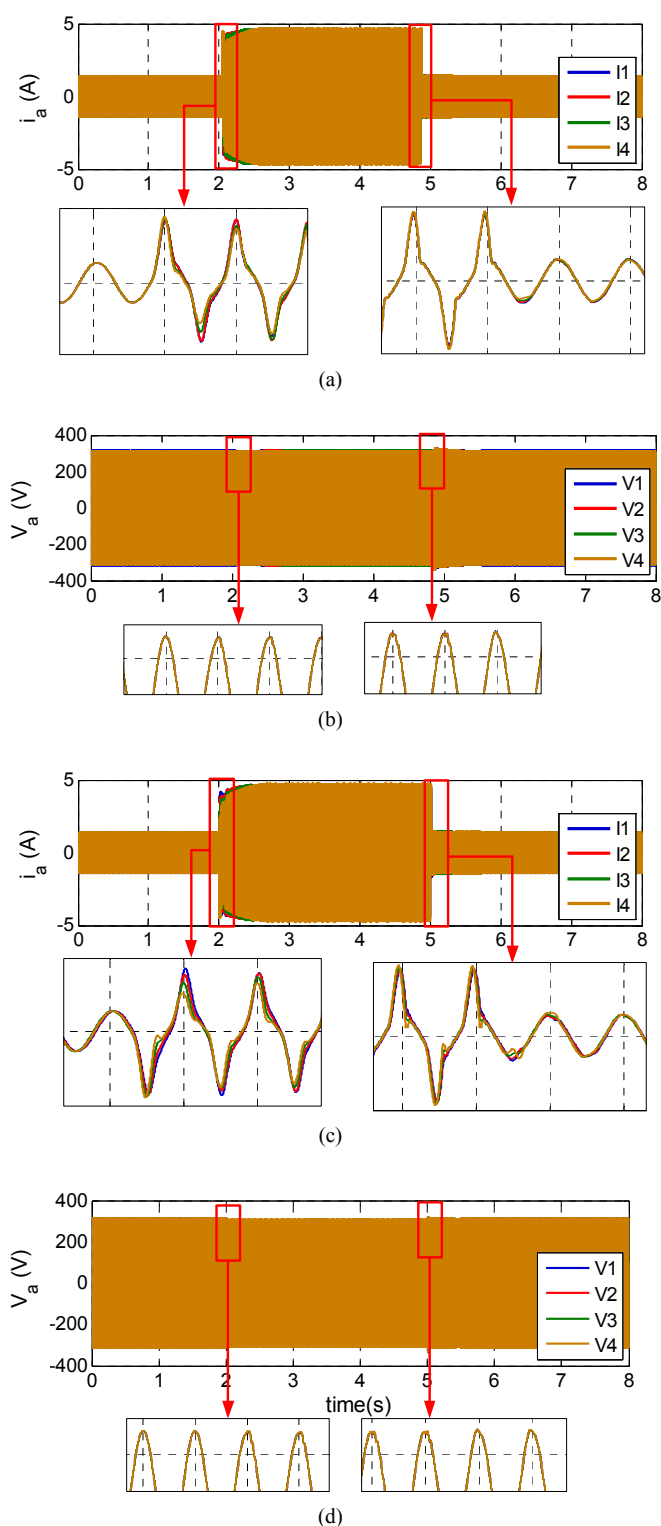


Fig. 12. Effect of network impedance on the performance of the proposed method: (a), (b) resistive network and (c), (d) inductive network.

#### E. Effect of communication delays

In the last case, the effect of communication delays on the step load response is studied. To that end, the communication delay is increased from 10ms to 100ms and 200ms and the step load change test is repeated. As shown in Fig. 13, although the increase of communication delay slows down the distributed secondary controller, but the proposed method exhibits an acceptable performance for delays of up to 200ms. It should be pointed out that modern communication technologies exhibit a much smaller delay (around 10-40ms) [44].

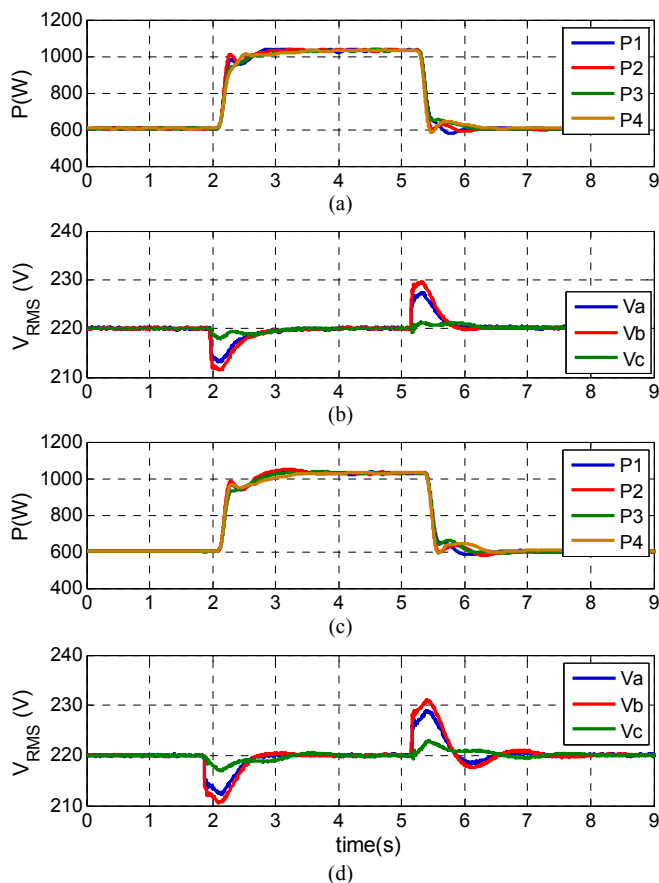


Fig. 13. Performance of proposed control method under different communication delays. (a) and (b) 100 ms (c) and (d) 200 ms.

## VI. CONCLUSIONS

The islanded MGs solely rely on the local DG units for voltage support and load/generation balance. On the other hand, the individual power electronic interfaced DG units have a relatively small capacity and are susceptible to overcurrent stresses. Therefore, an accurate load sharing strategy is crucial to prevent activating the overcurrent protection systems and possible damages.

In this paper, a new hierarchical control structure is proposed for improving power quality and current sharing accuracy of MGs. The control framework is comprised of primary level, which is responsible for fast and accurate sharing of instantaneous load current among the DG units and the secondary control, which facilitates accurate sharing of active power as well as compensating voltage distortions caused by nonlinear and unbalanced load currents. The proposed control framework takes advantage of GPS timing technology as a means for achieving fixed frequency operation and eliminating the transformation errors resulting from Park / inverse Park Transformations.

The proposed control architecture is independent of the system topology and does not require knowledge of line impedances. Since the current sharing is managed by the primary control level, which has a fast dynamic response, transient currents are also properly shared among the units. On the other hand, the large time constant of the secondary level enables implementation of the method with a low bandwidth communication network. Experimental results demonstrate the efficacy of the presented approach in terms of current sharing accuracy and power quality.

The proposed method is a forward step towards the integration of GPS technology with the state of the art control strategies in smart MGs. A future step is the incorporating of the GPS timing into grid connected control applications.

## REFERENCES

- [1] IEEE Guide for Design, Operation, and Integration of Distributed Resource Island Systems with Electric Power Systems, IEEE Standard 1547.4-2011, 2011.
- [2] J. M. Guerrero, M. Chandorkar, T. Lee, and P. C. Loh, "Advanced Control Architectures for Intelligent Microgrids ; Part I: Decentralized and Hierarchical Control," *IEEE Trans. Ind. Electron.*, vol. 60, pp. 1254-1262, April 2013.
- [3] L. Yun Wei and K. Ching-Nan, "An Accurate Power Control Strategy for Power-Electronics-Interfaced Distributed Generation Units Operating in a Low-Voltage Multibus Microgrid," *IEEE Trans. Power Electron.*, vol. 24, pp. 2977-2988, Dec. 2009.
- [4] J. M. Guerrero, V. Luis Garcia de, J. Matas, M. Castilla, and J. Miret, "Output Impedance Design of Parallel-Connected UPS Inverters With Wireless Load-Sharing Control," *IEEE Trans. Ind. Electron.*, vol. 52, pp. 1126-1135, Aug. 2005.
- [5] Y. A. R. I. Mohamed and E. F. El-Saadany, "Adaptive Decentralized Droop Controller to Preserve Power Sharing Stability of Paralleled Inverters in Distributed Generation Microgrids," *IEEE Trans. Power Electron.*, vol. 23, pp. 2806-2816, Nov. 2008.
- [6] J. M. Guerrero, J. Matas, V. Luis Garcia de, M. Castilla, and J. Miret, "Decentralized Control for Parallel Operation of Distributed Generation Inverters Using Resistive Output Impedance," *IEEE Trans. Ind. Electron.*, vol. 54, pp. 994-1004, Apr. 2007.
- [7] M. Savaghebi, J. C. Vasquez, A. Jalilian, J. M. Guerrero, and T. L. Lee, "Selective harmonic virtual impedance for voltage source inverters with LCL filter in microgrids," in *Energy Conversion Congress and Exposition (ECCE), 2012 IEEE*, 2012, pp. 1960-1965.
- [8] A. Micallef, M. Apap, C. Spiteri-Staines, and J. M. Guerrero, "Mitigation of Harmonics in Grid-Connected and Islanded Microgrids Via Virtual Admittances and Impedances," *IEEE Trans. Smart Grid*, p. Early access, 2015.
- [9] P. Sree Kumar and V. Khadkikar, "A New Virtual Harmonic Impedance Scheme for Harmonic Power Sharing in an Islanded Microgrid," *IEEE Trans. Power Del.*, vol. 31, pp. 936-945, June 2016.
- [10] M. Savaghebi, A. Jalilian, J. C. Vasquez, and J. M. Guerrero, "Secondary Control for Voltage Quality Enhancement in Microgrids," *IEEE Trans. Smart Grid*, vol. 3, pp. 1893-1902, Jul. 2012.
- [11] Y. Han, P. Shen, X. Zhao, and J. M. Guerrero, "Control Strategies for Islanded Microgrid Using Enhanced Hierarchical Control Structure With Multiple Current-Loop Damping Schemes," *IEEE Trans. Smart Grid*, Sept. 2015.
- [12] L. Meng, M. Savaghebi, F. Tang, T. Dragicevic, J. C. Vasquez, and J. M. Guerrero, "Dynamic consensus algorithm based distributed voltage harmonic compensation in islanded microgrids," in *Proc. European Conference on Power Electronics and Applications (EPE'15 ECCE-Europe)*, 2015, pp. 1-9.
- [13] J. He, Y. W. Li, and F. Blaabjerg, "An Enhanced Islanding Microgrid Reactive Power, Imbalance Power, and Harmonic Power Sharing Scheme," *IEEE Trans. Power Electron.*, vol. 30, pp. 3389-3401, June 2015.
- [14] H. Mahmood, D. Michaelson, and J. Jin, "Accurate Reactive Power Sharing in an Islanded Microgrid Using Adaptive Virtual Impedances," *IEEE Trans. Power Electron.*, vol. 30, pp. 1605-1617, March 2015.
- [15] M. Savaghebi, Q. Shafiee, J. C. Vasquez, and J. M. Guerrero, "Adaptive virtual impedance scheme for selective compensation of voltage unbalance and harmonics in microgrids," in *Proc. IEEE Power & Energy Society General Meeting*, 2015, pp. 1-5.
- [16] M. S. Golsorkhi and D. D. C. Lu, "A Control Method for Inverter-Based Islanded Microgrids Based on V-I Droop Characteristics," *IEEE Trans. Power Del.*, vol. 30, pp. 1196-1204, Jun. 2015.
- [17] M. LEXUAN, M. Savaghebi, T. Fen, T. Dragicevic, J. C. Vasquez, and J. M. Guerrero, "Dynamic consensus algorithm based distributed voltage harmonic compensation in islanded microgrids," in *Power Electronics and Applications (EPE'15 ECCE-Europe), 2015 17th European Conference on*, 2015, pp. 1-9.
- [18] M. S. Golsorkhi, D. D. C. Lu, M. Savaghebi, J. C. Vasquez, and J. M. Guerrero, "A GPS-based control method for load sharing and power quality improvement in microgrids," in *Proc. International Power Electronics and Motion Control Conference (IPEMC-ECCE Asia)*, 2016, pp. 3734-3740.

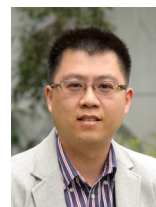
- [19] P. Rodriguez, A. Luna, I. Candela, R. Mujal, R. Teodorescu, and F. Blaabjerg, "Multiresonant Frequency-Locked Loop for Grid Synchronization of Power Converters Under Distorted Grid Conditions," *IEEE Trans. Ind. Electron.*, vol. 58, pp. 127-138, Jan. 2011.
- [20] M. Savaghebi, A. Jalilian, J. C. Vasquez, and J. M. Guerrero, "Secondary Control Scheme for Voltage Unbalance Compensation in an Islanded Droop-Controlled Microgrid," *IEEE Trans. Smart Grid*, vol. 3, pp. 797-807, Jun 2012.
- [21] Z. Zhian, X. Chunchun, B. J. Billian, Z. Li, S. S. Tsai, R. W. Conners, *et al.*, "Power system frequency monitoring network (FNET) implementation," *IEEE Trans. Power Syst.*, vol. 20, pp. 1914-1921, Nov. 2005.
- [22] E. M. Stewart, S. Kilicote, C. M. Shand, A. W. McMorran, R. Arghandeh, and A. v. Meier, "Addressing the challenges for integrating micro-synchrophasor data with operational system applications," in *Proc. IEEE PES General Meeting*, 2014, pp. 1-5.
- [23] A. H. Etemadi, E. J. Davison, and R. Iravani, "A Decentralized Robust Control Strategy for Multi-DER Microgrids - Part I: Fundamental Concepts," *IEEE Trans. Power Del.*, vol. 27, pp. 1843-1853, Sept. 2012.
- [24] S. Rivero, F. Sarzo, and G. Ferrari-Trecate, "Plug-and-Play Voltage and Frequency Control of Islanded Microgrids With Meshed Topology," *IEEE Trans. Smart Grid*, vol. 6, pp. 1176-1184, May 2015.
- [25] R. Majumder, A. Ghosh, G. Ledwich, and F. Zare, "Angle droop versus frequency droop in a voltage source converter based autonomous microgrid," in *Proc. IEEE PES General Meeting*, 2009, pp. 1-8.
- [26] M. S. Golsorkhi and D. D. C. Lu, "A decentralized power flow control method for islanded microgrids using V-I droop," in *Proc. Iranian Conference on Electrical Engineering (ICEE)*, 2014, pp. 604-609.
- [27] M. S. Golsorkhi, Q. Shafiee, D. Lu, and J. M. Guerrero, "A Distributed Control Framework for Integrated Photovoltaic-Battery Based Islanded Microgrids," *IEEE Trans. Smart Grid*, Early Access (DOI: 10.1109/TSG.2016.2593030), 2016.
- [28] M. S. Golsorkhi and D. D. C. Lu, "A decentralized negative sequence compensation method for islanded microgrids," in *Proc. International Symposium on Power Electronics for Distributed Generation Systems (PEDG)*, 2015, pp. 1-7.
- [29] M. Golsorkhi, D. Lu, and J. Guerrero, "A GPS-Based Decentralized Control Method for Islanded Microgrids," *IEEE Trans. Power Electron.*, (DOI: 10.1109/TPEL.2016.2551265), April 2016.
- [30] M. S. Golsorkhi and D. D. C. Lu, "A Decentralized Control Method for Islanded Microgrids Under Unbalanced Conditions," *IEEE Trans. Power Del.*, vol. 31, pp. 1112-1121, Jun. 2016.
- [31] Y. Quan and G. Liu, "Compensation Local Clock\_s Drift by Timestamp Stream," in *Proc. Innovative Computing, Information and Control*, 2007, pp. 524-524.
- [32] J. M. Guerrero, J. C. Vasquez, J. Matas, V. de, L. G. a, and M. Castilla, "Hierarchical Control of Droop-Controlled AC and DC Microgrids, A General Approach Toward Standardization," *IEEE Trans. Ind. Electron.*, vol. 58, pp. 158-172, Jan. 2011.
- [33] C. D. Presti, F. Carrara, A. Scuderi, and G. Palmisano, "Fast Peak Detector with Improved Accuracy and Linearity for High-Frequency Waveform Processing," in *Proc. IEEE International Symposium on Circuits and Systems (ISCAS)*, 2007, pp. 3884-3887.
- [34] R. Olfati-Saber, J. A. Fax, and R. M. Murray, "Consensus and Cooperation in Networked Multi-Agent Systems," *Proc.*, vol. 95, pp. 215-233, Jan. 2007.
- [35] J. W. Simpson-Porco, Q. Shafiee, F. Dorfler, J. C. Vasquez, J. M. Guerrero, and F. Bullo, "Secondary Frequency and Voltage Control of Islanded Microgrids via Distributed Averaging," *IEEE Trans. Ind. Electron.*, vol. 62, pp. 7025-7038, Nov. 2015.
- [36] M. Savaghebi, A. Jalilian, J. C. Vasquez, and J. M. Guerrero, "Secondary control for voltage quality enhancement in microgrids," *IEEE Trans. Smart Grid*, vol. 3, no. 4, pp. 1893-1902, Dec 2012.
- [37] T. G. Kolda, R. M. Lewis, and V. Torczon, "Optimization by direct search: New perspectives on some classical and modern methods," *SIAM review*, vol. 45, pp. 385-482, 2003.
- [38] L. Yunwei, D. M. Vilathgamuwa, and L. Poh Chiang, "Microgrid power quality enhancement using a three-phase four-wire grid-interfacing compensator," *IEEE Trans. Ind. Appl.*, vol. 41, pp. 1707-1719, Nov. 2005.
- [39] Q. Shafiee, J. M. Guerrero, and J. C. Vasquez, "Distributed Secondary Control for Islanded Microgrids-A Novel Approach," *IEEE Trans. Power Electron.*, vol. 29, pp. 1018-1031, Feb. 2014.
- [40] L. Meng, A. Luna, D. E. R. x00Ed, az, B. Sun, *et al.*, "Flexible System Integration and Advanced Hierarchical Control Architectures in the Microgrid Research Laboratory of Aalborg University," *IEEE Trans. Ind. Appl.*, vol. 52, pp. 1736-1749, Mar. 2016.
- [41] M. Liserre, F. Blaabjerg, and S. Hansen, "Design and control of an LCL-filter-based three-phase active rectifier," *IEEE Trans. Ind. Appl.*, vol. 41, pp. 1281-1291, Sept. 2005.
- [42] J. Muhlethaler, M. Schweizer, R. Blattmann, J. W. Kolar, and A. Ecklebe, "Optimal Design of LCL Harmonic Filters for Three-Phase PFC Rectifiers," *IEEE Trans. Power Electron.*, vol. 28, pp. 3114-3125, July 2013.
- [43] A. Engler and N. Soultanis, "Droop control in LV-grids," in *Future Power Systems, 2005 International Conference on*, 2005, pp. 6 pp.-6.
- [44] M. A. G. Sayani, B. K. Singh, J. Coulter, and K. E. Tepe, "Segment wise communication delay measurement for Smart Grid applications," in *Communications (QBSC), in Symposium on Biennial*, 2014, pp. 139-143.



**Mohammad S. Golsorkhi** (S'13) received the B.Sc. (Hons.) degree in electrical engineering from Isfahan University of Technology, Isfahan, Iran, in 2009 and the M.Sc. (Hons.) degree in electrical engineering from Tehran Poly-technique, Tehran, Iran, in 2012. During 2011-2012, he worked in Behrad consulting engineers as a R&D engineer. He is currently pursuing the PhD degree in electrical engineering at The University of Sydney, Australia. In 2015, he was a visiting PhD student with the Department of Energy Technology, Aalborg University, Denmark. His current research interests include control of microgrids, renewable energy resources, and power electronics.



**Mehdi Savaghebi** (S'06-M'15-SM'15) received the B.Sc. degree from University of Tehran, Iran, in 2004 and the M.Sc. and Ph.D. degrees with highest honors from Iran University of Science and Technology, Tehran, Iran in 2006 and 2012, respectively, all in Electrical Engineering. From 2007 to 2014, he was a Lecturer in Electrical Engineering Department, Karaj Branch, Islamic Azad University. Currently, he is a Postdoctoral Fellow in the Department of Energy Technology, Aalborg University. His main research interests include distributed generation systems, microgrids, power quality and smart metering. Dr. Savaghebi is a member of Technical Committee of Renewable Energy Systems, IEEE Industrial Electronics Society and also IEEE Task Force on Microgrids Stability Analysis and Modeling.



**Dylan Dah-Chuan Lu** (M'04-SM'09) received his Ph.D. degree from The Hong Kong Polytechnic University, Hong Kong, in 2004. In 2003, he joined PowerLab Ltd. as a Senior Design Engineer and worked on industrial switching power supply projects. He was a faculty member with The University of Sydney from 2006 to 2016. Since July 2016, he is an Associate Professor at the School of Electrical, Mechanical and Mechatronic Systems, University of Technology, Sydney, Australia. His current research interests include power electronics for renewable energy systems and microgrids. He is a member of Engineers Australia. He was the recipient of the Best Paper Award in the category of Emerging Power Electronic Technique at the *IEEE PEDS* 2015. He presently serves as an Associate Editor of the *IEEE Transactions on Circuits and Systems II* and the *IET Renewable Power Generation*.



**Josep M. Guerrero** (S'01-M'04-SM'08-FM'15) received the B.S. degree in telecommunications engineering, the M.S. degree in electronics engineering, and the Ph.D. degree in power electronics from the Technical University of Catalonia, Barcelona, in 1997, 2000 and 2003, respectively. Since 2011, he has been a Full Professor with the Department of Energy Technology, Aalborg University, Denmark, where he is responsible for the Microgrid Research Program.



**Juan C. Vasquez** (M'12-SM'14) received the B.S. degree in electronics engineering from the Autonomous University of Manizales, Colombia, and the Ph.D. degree from UPC, Barcelona, Spain, in 2004 and 2009, respectively. In 2011, he was Assistant Professor and from 2014 he is working as a Tenured Associate Professor at AAU, Denmark where he is the Vice Programme Leader of the Microgrids Program. His current research interests include Microgrids and the integration of Internet of Things and Cyber-Physical Systems into the SmartGrid. Dr. Vasquez is a member of the IEC Evaluation Group SEG4 on LVDC, PELS, IAS, and PES Societies.